Significant Structural Disorganization in Alkaline Molybdenum(V) Aluminophosphates

A. Guesdon, A. Leclaire,* M. M. Borel, and B. Raveau

Laboratoire CRISMAT, ISMRA et Université de Caen, Boulevard du Maréchal Juin 14050, Caen Cedex, France

Received March 14, 1995. Revised Manuscript Received August 3, 1995[⊗]

Three new molybdenum(V) aluminophosphates, $K_2Cs_7Mo_9Al_3P_{11}O_{59}$, $K_4Cs_5Mo_9Al_3P_{11}O_{59}$, and $Rb_9Mo_9Al_3P_{11}O_{59}$, isotypic with the tunnel structure $Cs_9Mo_9Al_3P_{11}O_{59}$, have been synthesized. Their single-crystal X-ray diffraction study evidences high thermal factors for most of the atoms and splittings of several sites which are interpreted as a significant disorganization of the framework $[Mo_9Al_3P_{11}O_{59}]_\infty$, resulting from various tiltings of the chains of polyhedra rather than from a distortion of the latter. The second important feature deals with the distribution of the interpolated A cations in the tunnels: exclusive occupancy of the large tunnels by cesium ions, whereas the potassium ions are located in the smaller ones, and existence of additional sites for Rb^+ in $Rb_9Mo_9Al_3P_{11}O_{59}$. The abnormally large A–O distances are also discussed in connection with the high thermal factors observed for the A^+ cations.

Introduction

In the large field of Mo(V) phosphates (see for a review refs 1 and 2), very few Mo(V) aluminophosphates are known to date. After the synthesis of the phase $MoAlP_2O_9$,[3] the recent exploration of the system Cs–Mo–Al–P–O has allowed a second molybdenum(V) aluminophosphate, $Cs_9Mo_9Al_3P_{11}O_{59}$,[4] to be isolated. The hexagonal structure of this phase exhibits two kinds of tunnels where the cesium cations are located. The most striking characteristic of this structure deals with the very large size of one kind of tunnels which are in fact bordered by the oxygen atoms of the molybdenyl groups. Moreover, the Cs^+ cations that belong to these larger tunnels are located near the walls and exhibit abnormally large Cs–O distances ranging from 3.11 to 3.37 Å, which explain the high thermal factors of about 3.7 Å^2 obtained for these cations. To understand the influence of the interpolated cation on the stability of this framework and on its structural evolution and also to study the possibility that migration of small cations through the large tunnels could give rise to ionic conduction, we have investigated the substitution of potassium and rubidium for cesium in this Mo(V) aluminophosphate, trying to grow single crystals. We report here on the crystal structure study of three oxides, $K_2Cs_7Mo_9Al_3P_{11}O_{59}$, $K_4Cs_5Mo_9Al_3P_{11}O_{59}$, and $Rb_9Mo_9Al_3P_{11}O_{59}$, that are isotypic with $Cs_9Mo_9Al_3P_{11}O_{59}$ but which show a significant disorganization of the structure.

Experimental Section

Synthesis and Characterization. The synthesis of the different compounds was performed under the same conditions as those used for $Cs_9Mo_9Al_3P_{11}O_{59}$,[4] i.e., in two steps. First, a mixture of $H(NH_4)_2PO_4$, $Al(NO_3)_3{\cdot}9H_2O$, MoO_3, and a nitrate or a carbonate of the particular alkaline cation was heated up to 673 K in air in order to decompose the nitrate or carbonate and the ammonium phosphate. In the second step, the resulting finely ground powder was mixed with the appropriate amount of molybdenum (0.66 mol). This sample, placed in an alumina tube, was sealed in an evacuated silica ampule, heated to 1000 K for 2 days and quenched to room temperature.

Attempts to synthesize $A_9Mo_9Al_3P_{11}O_{59}$ were successful for A = Rb and unsuccessful for A = Na, K, and Tl. The $K_xCs_{9-x}Mo_9Al_3P_{11}O_{59}$ compounds were obtained for $x \leq 4$. Finally, the $Rb_xCs_{9-x}Mo_9Al_3P_{11}O_{59}$ compounds were synthesized for x ranging from 0 to 9.

The powder X-ray diffraction patterns of these phases were indexed in a hexagonal cell in agreement with the parameters obtained from the single-crystal study (Table 1), showing their isotypism with the $Cs_9Mo_9Al_3P_{11}O_{59}$ structure.

Crystals were grown in a similar way as described above, but the samples were heated to 1050 K for 1 day, then slowly cooled at 2 K h^{-1} to 920 K and finally quenched to room temperature. Orange single crystals were extracted from different batches. The refinement of their crystal structure confirmed they were isotypic with $Cs_9Mo_9Al_3P_{11}O_{59}$ and was in agreement with the molar ratios obtained for each of them by microprobe analysis.

Structure Determination. Four orange crystals with dimensions 0.212 × 0.167 × 0.077 mm, 0.129 × 0.051 × 0.051 mm, 0.141 × 0.141 × 0.103 mm, and 0.071 × 0.026 × 0.026 mm for $Rb_9Mo_9Al_3P_{11}O_{59}$, $K_2Cs_7Mo_9Al_3P_{11}O_{59}$, $K_4Cs_5Mo_9Al_3P_{11}O_{59}$, and $Rb_4Cs_5Mo_9Al_3P_{11}O_{59}$, respectively, were selected. Their cell parameters, reported in Table 1, were determined and refined by diffractometric techniques at 294 K with a least-squares refinement based upon 25 reflections with $18° < \theta < 22°$. The $Rb_4Cs_5Mo_9Al_3P_{11}O_{59}$ crystal was too small to allow a structure resolution. The structure determinations of the

Table 1. Cell Parameters

compounds	a (Å)	c (Å)	V (Å^3)
$Cs_9Mo_9Al_3P_{11}O_{59}$	16.989 (3)	11.866 (3)	2966 (2)
$Rb_9Mo_9Al_3P_{11}O_{59}$	16.710 (2)	11.900 (2)	2878 (1)
$K_2Cs_7Mo_9Al_3P_{11}O_{59}$	16.952 (2)	11.833 (1)	2945 (1)
$K_4Cs_5Mo_9Al_3P_{11}O_{59}$	16.832 (4)	11.796 (2)	2894 (2)
$Rb_4Cs_5Mo_9Al_3P_{11}O_{59}$	16.891 (5)	11.769 (9)	2908 (3)

[⊗] Abstract published in *Advance ACS Abstracts,* September 1, 1995.

(1) Haushalter, R. C.; Mundi, L. A. *Chem. Mat.* **1992**, *4*, 31.
(2) Costentin, G.; Leclaire, A.; Borel, M. M.; Grandin, A.; Raveau, B. *Rev. Inorg. Chem.* **1993**, *13*, 77.
(3) Leclaire, A.; Borel, M. M.; Grandin, A.; Raveau, B. *Z. Kristallogr.* **1990**, *190*, 135–142.
(4) Guesdon, A.; Borel, M. M.; Leclaire, A.; Grandin, A.; Raveau, B. *J. Solid State Chem.* **1995**, *114*, 451.

0897-4756/95/2807-1873$09.00/0

Table 2. Summary of Intensity Measurements and Structure Refinement parameters

	$K_2Cs_7Mo_9Al_3P_{11}O_{59}$	$K_4Cs_5Mo_9Al_3P_{11}O_{59}$	$Rb_9Mo_9Al_3P_{11}O_{59}$
	Intensity Measurements		
λ (Mo Kα)	0.710 73	0.710 73	0.710 73
scan mode	$\omega-{}^2/_3\theta$	$\omega-\theta$	$\omega-{}^2/_3\theta$
scan width (deg)	1.50 + 0.35 tan θ	1.17 + 0.35 tan θ	1.60 + 0.35 tan θ
slit aperture (mm)	1.50 + tan θ	1.12 + tan θ	1.40 + tan θ
max θ (deg)	45	45	45
standard reflns	3 every 3 000 s (no decay)	3 every 3 000 s (no decay)	3 every 3 000 s (no decay)
reflns with $I > 2.5\sigma$	1223	1271	922
reflns measd	8887	8716	8662
μ (mm^{-1})	6.65	5.68	9.69
	Structure Solution and Refinement		
parameters refined	110	110	134
agreement factors	$R = 0.043$ $R_w = 0.040$	$R = 0.067$ $R_w = 0.077$	$R = 0.062$ $R_w = 0.067$
weighting scheme	$w = f(\sin\theta/\lambda)$	$w = f(\sin\theta/\lambda)$	$w = f(\sin\theta/\lambda)$
Δ/σ(max)	<0.004	<0.004	<0.03
$\Delta\varrho$ (e Å^{-3})	<2.2	<4.6	<1.9

three other crystals were performed in the $P6_3/m$ centrosymmetric space group (as for $Cs_9Mo_9Al_3P_{11}O_{59}$) in agreement with the observed systematic absence $l = 2n + 1$ for $00l$. The data were collected on a CAD4 Enraf-Nonius diffractometer with the data collection parameters of Table 2. The reflections were corrected for Lorentz and polarization effects; absorption corrections were performed for the $Rb_9Mo_9Al_3P_{11}O_{59}$ and $K_2Cs_7Mo_9Al_3P_{11}O_{59}$ crystals. The three structures were solved by the heavy-atom method. The Patterson functions confirmed that those three aluminophosphates were isotypic with $Cs_9Mo_9Al_3P_{11}O_{59}$. Thus the refinements of the structures were started from the atomic coordinates of $Cs_9Mo_9Al_3P_{11}O_{59}$. Refinement of the atomic coordinates, of the anisotropic thermal factors for Mo, P, Al, and for the alkali cations and of the isotropic thermal factors for the oxygen atoms led to $R = 0.043$ and $R_w = 0.040$ for $K_2Cs_{15}Mo_9Al_3P_{11}O_{59}$, to $R = 0.067$ and $R_w = 0.077$ for $K_4Cs_{15}Mo_9Al_3P_{11}O_{59}$ and to $R = 0.062$ and $R_w = 0.067$ for $Rb_9Mo_9Al_3P_{11}O_{59}$. The atomic parameters resulting from the refinements are reported in Table 3.

The rather high values of the R factors for the two latter compounds are due to the high standard deviations of the F_o, resulting from the weakness of the diffraction spots.

Description of the Structure and Discussion

If one disregards the abnormally high isotropic thermal factors of the atoms, which will be discussed later, the structure of these compounds is very similar to that of $Cs_9Mo_9Al_3P_{11}O_{59}$.[4] As shown from the projection of the structure along $\vec{c}$ (Figure 1), the $[Mo_9Al_3P_{11}O_{59}]_\infty$ framework consists indeed of corner-sharing AlO_4 and PO_4 tetrahedra and MoO_6 octahedra forming $[AlMo_3P_3O_{22}]_\infty$ columns linked through their apexes. This host lattice delimits two sorts of tunnels running along $\vec{c}$,

Table 3. Positional Parameters and Their Estimated Standard Deviations[a]

atom	x	y	z	B (Å^2)	site	occupancy	atom	x	y	z	B (Å^2)	site	occupancy
						$K_2Cs_7Mo_9Al_3P_{11}O_{59}$							
K_1C_2[b]	0.14585(8)	0.52661(9)	0.4524(1)	3.08(2)	12i	1	O(4)	0.2869(5)	0.4478(5)	0.4209(7)	1.3(1)*	12i	1
Cs(2)	0.02728(9)	0.1981(1)	0.2632(4)	4.43(5)	12i	0.5	O(5)	0.4139(7)	0.4826(7)	0.25	1.5(2)*	6h	1
Mo(1)	0.27303(8)	0.44149(8)	0.25	0.79(2)	6h	1	O(6)	0.1704(6)	0.1495(6)	0.3772(9)	2.7(2)*	12i	1
Mo(2)	0.27964(6)	0.23429(6)	0.36063(9)	1.16(2)	12i	1	O(7)	0.2720(5)	0.3037(5)	0.5025(8)	1.8(2)*	12i	1
P(1)	0.4486(3)	0.4133(3)	0.25	1.19(9)	6h	1	O(8)	0.3412(5)	0.1936(5)	0.4767(8)	2.1(2)*	12i	1
P(2)	0.3785(2)	0.1285(2)	0.4822(2)	0.96(5)	12i	1	O(9)	0.3192(8)	0.1776(8)	0.25	1.8(2)*	6h	1
P(3)	0.66667	0.33333	0.7135(9)	1.3(2)	4f	0.5	O(10)	0.4147(5)	0.3543(5)	0.3554(7)	1.6(1)*	12i	1
P(4)	0.33333	0.66667	0.700(1)	1.6(2)	4f	0.5	O(11)	0.5533(8)	0.4684(9)	0.25	2.6(3)*	6h	1
Al	0.4871(3)	0.1557(3)	0.25	1.0(1)	6h	1	O(12)	0.4299(6)	0.1317(6)	0.3765(8)	2.5(2)*	12i	1
O(1)	0.1615(8)	0.4079(8)	0.25	2.0(2)*	6h	1	O(13)	0.66667	0.33333	0.587(3)	2.1(6)*	4f	0.5
O(2)	0.3193(8)	0.5756(9)	0.25	2.4(3)*	6h	1	O(14)	0.3039(9)	0.5738(9)	0.75	3.0(3)*	6h	1
O(3)	0.2548(7)	0.3115(7)	0.25	1.1(2)*	6h	1	O(15)	0.33333	0.66667	0.573(4)	3.6(8)*	4f	0.5
						$K_4Cs_5Mo_9Al_3P_{11}O_{59}$							
K_2C_1[c]	0.1442(2)	0.5255(2)	0.4518(2)	3.94(5)	12i	1	O(4)	0.2888(8)	0.4488(9)	0.421(1)	2.5(2)*	12i	1
Cs(2)	0.0293(2)	0.2011(2)	0.2679(6)	7.0(1)	12i	0.5	O(5)	0.419(1)	0.485(1)	0.25	2.5(4)*	6h	1
Mo(1)	0.2757(1)	0.4436(1)	0.25	1.24(3)	6h	1	O(6)	0.173(1)	0.149(1)	0.375(2)	5.1(4)*	12i	1
Mo(2)	0.2819(1)	0.23553(9)	0.3607(2)	2.21(3)	12i	1	O(7)	0.274(1)	0.307(1)	0.503(2)	3.4(3)*	12i	1
P(1)	0.4513(4)	0.4144(5)	0.25	1.9(1)	6h	1	O(8)	0.344(1)	0.194(1)	0.478(1)	3.4(3)*	12i	1
P(2)	0.3807(3)	0.1296(3)	0.4832(4)	1.51(8)	12i	1	O(9)	0.320(1)	0.179(1)	0.25	3.1(4)*	6h	1
P(3)	0.66667	0.33333	0.719(1)	1.1(1)	4f	0.5	O(10)	0.4178(9)	0.3560(9)	0.357(1)	2.6(3)*	12i	1
P(4)	0.33333	0.66667	0.684(1)	1.8(2)	4f	0.5	O(11)	0.555(2)	0.466(2)	0.25	5.3(6)*	6h	1
Al	0.4863(5)	0.1578(5)	0.25	1.5(1)	6h	1	O(12)	0.431(1)	0.133(1)	0.378(2)	5.5(5)*	12i	1
O(1)	0.166(1)	0.412(1)	0.25	2.8(4)*	6h	1	O(13)	0.66667	0.33333	0.601(5)	3(1)*	4f	0.5
O(2)	0.324(2)	0.577(2)	0.25	4.7(6)*	6h	1	O(14)	0.301(2)	0.574(2)	0.75	4.1(5)*	6h	1
O(3)	0.257(1)	0.312(1)	0.25	2.1(3)*	6h	1	O(15)	0.33333	0.66667	0.561(5)	3(1)*	4f	0.5
						$Rb_9Mo_9Al_3P_{11}O_{59}$							
Rb(1)	0.1507(2)	0.5317(2)	0.4578(2)	4.03(5)	12i	0.95	O(3)	0.256(1)	0.311(1)	0.25	1.4(3)*	6h	1
Rb(2a)	0.0300(6)	0.2153(8)	0.2807(8)	5.0(3)	12i	0.25	O(4)	0.2894(9)	0.452(1)	0.419(1)	3.2(3)*	12i	1
Rb(2b)	0.0375(6)	0.1800(8)	0.354(1)	5.8(3)	12i	0.25	O(5)	0.416(1)	0.486(1)	0.25	2.6(4)*	6h	1
Rb(3)	0.0	0.0	0.5	4.6(4)	2b	0.30	O(6a)	0.194(2)	0.153(2)	0.375(3)	3.4(7)*	12i	0.5
Mo(1)	0.2730(2)	0.4424(2)	0.25	1.71(5)	6h	1	O(6b)	0.155(2)	0.152(2)	0.371(3)	4.7(8)	12i	0.5
Mo(2a)	0.2732(2)	0.2293(2)	0.3566(3)	2.20(6)	12i	0.5	O(7)	0.276(1)	0.309(1)	0.500(2)	4.1(4)*	12i	1
Mo(2b)	0.2969(2)	0.2448(2)	0.3621(3)	2.25(7)	12i	0.5	O(8)	0.349(1)	0.201(1)	0.480(2)	5.3(4)*	12i	1
P(1)	0.4522(5)	0.4174(7)	0.25	3.0(2)	6h	1	O(9)	0.328(2)	0.183(2)	0.25	5.7(7)*	6h	1
P(2)	0.3815(3)	0.1306(3)	0.4842(4)	1.9(1)	12i	1	O(10)	0.4202(9)	0.3589(9)	0.357(1)	3.0(3)*	12i	1
P(3)	0.66667	0.33333	0.718(1)	1.5(4)	4f	0.5	O(11)	0.557(2)	0.471(2)	0.25	7.6(9)*	6h	1
P(4)	0.33333	0.66667	0.692(2)	3.5(3)	4f	0.5	O(12)	0.434(1)	0.134(1)	0.380(2)	5.3(4)*	12i	1
Al	0.4813(6)	0.1551(5)	0.25	2.9(2)	6h	1	O(13)	0.66667	0.33333	0.589(4)	2.0(9)*	4f	0.5
O(1)	0.159(2)	0.401(2)	0.25	4.2(5)*	6h	1	O(14)	0.302(2)	0.572(2)	0.75	5.8(7)*	6h	1
O(2)	0.315(2)	0.576(2)	0.25	6.6(8)*	6h	1	O(15)	0.33333	0.66667	0.573(5)	3(1)*	4f	0.5

[a] Starred atoms were refined isotropically. Anisotropically refined atoms are given in the form of the isotropic equivalent displacement parameter defined as $B = {}^4/_3\sum_i\sum_j \vec{a}_i\vec{a}_j\beta_{ij}$. [b] ${}^1/_3$ K, ${}^2/_3$ Cs. [c] ${}^2/_3$ K, ${}^1/_3$ Cs.

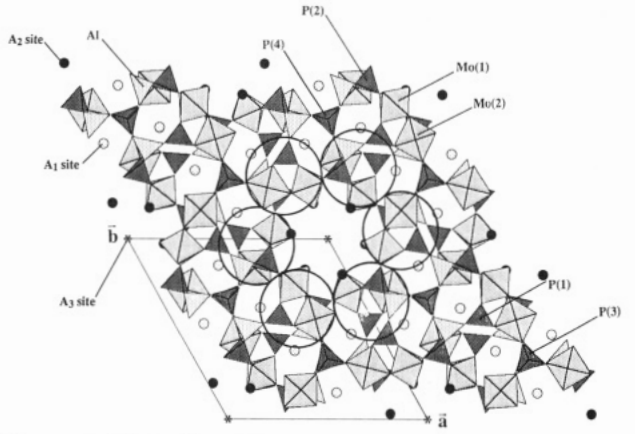

Figure 1. Projection of the structure along $\vec{c}$ showing the two kinds of tunnels and the $[AlMo_3P_3O_{22}]_\infty$ columns (circled).

Table 4. Distances (Å) in the Polyhedra

	$Cs_9Mo_9Al_3P_{11}O_{59}$	$Rb_9Mo_9Al_3P_{11}O_{59}$	$K_2Cs_7Mo_9Al_3P_{11}O_{59}$	$K_4Cs_5Mo_9Al_3P_{11}O_{59}$
Mo(1)−O(1)	1.670(7)	1.66(3)	1.68(1)	1.65(2)
−O(2)	2.014(8)	1.98(4)	2.00(2)	1.97(3)
−O(3)	2.051(7)	2.07(2)	2.07(1)	2.08(2)
−O(4)	2.015(5)	2.02(2)	2.032(8)	2.03(1)
−O(5)	2.129(7)	2.12(2)	2.13(1)	2.15(2)
Mo(2)−O(3)	2.051(5)	2.03(3)[a]	2.038(9)	2.02(2)
−O(6)	1.696(6)	1.69(5)[a]	1.70(1)	1.68(2)
−O(7)	2.079(5)	2.12(4)[a]	2.091(9)	2.10(2)
−O(8)	2.047(5)	2.07(4)[a]	2.04(1)	2.05(2)
−O(9)	1.920(6)	1.93(4)[a]	1.93(1)	1.90(2)
−O(10)	2.170(5)	2.16(4)[a]	2.174(8)	2.17(2)
P(1)−O(5)	1.542(7)	1.55(3)	1.56(1)	1.54(2)
−O(10)	1.528(5)	1.53(2)	1.520(9)	1.52(2)
−O(11)	1.531(8)	1.51(4)	1.54(2)	1.52(3)
P(2)−O(4)	1.550(5)	1.55(2)	1.533(9)	1.50(2)
−O(7)	1.509(5)	1.48(2)	1.500(9)	1.49(2)
−O(8)	1.518(5)	1.52(2)	1.52(1)	1.49(2)
−O(12)	1.510(6)	1.50(2)	1.51(1)	1.49(2)
P(3)−O(2)	1.506(8)	1.44(4)	1.50(1)	1.48(3)
−O(13)	1.49(2)	1.53(6)	1.50(4)	1.40(6)
P(4)−O(14)	1.522(8)	1.55(3)	1.52(2)	1.58(3)
−O(15)	1.50(3)	1.42(7)	1.50(5)	1.45(6)
Al−O(11)	1.738(8)	1.70(4)	1.71(2)	1.70(3)
−O(12)	1.730(6)	1.69(2)	1.72(1)	1.71(2)
−O(14)	1.715(9)	1.75(4)	1.75(2)	1.74(3)

[a] Average value of the distances in the Mo(2a)−O_6 and Mo(2b)−O_6 octahedra.

small six-sided tunnels and very large tunnels formed by crowns of 12 octahedra, both occupied by alkali cations.

As in $Cs_9Mo_9Al_3P_{11}O_{59}$, the two MoO_6 octahedra exhibit in these alumino phosphates a free corner and present the same geometry (characteristic of molybdenum V), i.e., a very short Mo−O bond (from 1.65 to 1.68 Å for Mo(1)−O(1) and from 1.68 to 1.70 Å for Mo(2)−O(6)) and an opposite abnormally long Mo−O bond (from 2.12 to 2.15 Å for Mo(1)−O(5) and from 2.16 to 2.17 Å for Mo(2)−O(10)). The four other distances are intermediate (ranging from 1.97 to 2.08 Å in $Mo(1)O_6$ and from 1.90 to 2.12 Å in $Mo(2)O_6$) (Table 4). The valence calculations according to Zachariasen[5] confirm the pentavalent character of the two molybdenum atoms in these compounds (Table 5).

The geometry of the tetrahedra is similar to those usually observed, with Al−O distances ranging from 1.69 to 1.75 Å and P−O distances between 1.42 and 1.58 Å. Like in $Cs_9Mo_9Al_3P_{11}O_{59}$, the P(3) and P(4) tetrahedra are in these frameworks statistically distributed over two split half-occupied positions.

Table 5. Valence Calculations

	$Cs_9Mo_9Al_3P_{11}O_{59}$	$Rb_9Mo_9Al_3P_{11}O_{59}$	$K_2Cs_7Mo_9Al_3P_{11}O_{59}$	$K_4Cs_5Mo_9Al_3P_{11}O_{59}$
Mo(1)	5.1	5.1	4.9	5.2
Mo(2)	4.9	4.9[a]	4.9	5.1

[a] Average value calculated from the distances reported in Table 4.

The first important difference between these structures and that of the Cs phase deals with the very high B_{eq} and B factors observed for several atoms other than the interpolated cations (Table 3). It is remarkable that the B factors of almost all the atoms increase significantly and sometimes dramatically as the cesium content decreases.

This phenomenon is connected with the quasi-absence of reflections for $\theta > 31°$. It can be explained by a significant disorganization of the framework due to the introduction of smaller cations which do not fit with the large size of the tunnels and consequently favor either the thermal agitation of the atoms or allow multiple local distortions of the groups of polyhedra. Unfortunately, the refinement of the anisotropic factors cannot be performed on the oxygen atoms owing to the too small number of observed reflections whatever the size of the sample. The "K_2Cs_7" crystal has 1223 reflections with $I > 2.5\sigma(I)$, whereas the "K_4Cs_5" sample, which is 6 times larger, has only 48 more reflections; moreover, the "Rb_9" crystal is 8 times larger than the "K_2Cs_7", but it has only 922 reflections, i.e., 301 (25%) less than the "K_2Cs_7" crystal. Nevertheless, the refinement of the anisotropic factors of the molybdenum atoms (Table 6) clearly establishes that one of these Mo(2) exhibits a high agitation directed toward the center of the 12-sided tunnels. This agitation increases as the cesium content decreases, so that for the pure rubidium phase, $Rb_9Mo_9Al_3P_{11}O_{59}$, the Mo(2) atoms have been split into two half-occupied positions; in the same way the O(6) atom that forms the molybdenyl group with Mo(2) had to be split into two positions for the same reason (Table 3). In other words, one observes at least two kinds of tiltings of the octahedral Mo_3O_{15} units in the rubidium phase $Rb_9Mo_9Al_3P_{11}O_{59}$. Such tiltings of the polyhedra should in fact imply superstructures, if one admits that the chains of polyhedra cannot be tilted completely at random with respect to each other but rather in a concerted way to avoid strains. The Weissenberg and rotating crystal patterns of $Rb_9Mo_9Al_3P_{11}O_{59}$ support strongly this viewpoint: one indeed observes additional reflections that imply a doubling of the "a" and "c" parameters. Unfortunately, the resolution of the actual structure is made impossible by the too low number of superstructure spots despite of the large size of the sample. To study further this very weak superstructure, a transmission electron microscope was used. Under the electron beam, the superstructure disappeared so quickly that no recording of the diffraction patterns was possible to allow a study of the actual space group. This space group must be trigonal instead of hexagonal in the subcell, to avoid a binary axis or binary screw axis in the large tunnels.

The second important feature deals with the distribution of the alkali ions in the tunnels and with their thermal agitation. One first observes that the smaller six-sided tunnels are preferentially occupied by potassium in both aluminophosphates, $K_2Cs_7Mo_9Al_3P_{11}O_{59}$

Table 6. Anisotropic Thermal Factors[a]

Name	β_{11}	β_{22}	β_{33}	β_{12}	β_{13}	β_{23}
			$K_2Cs_7Mo_9Al_3P_{11}O_{59}$			
K_1C_2	0.00632(4)	0.00387(3)	0.00406(7)	0.00826(5)	0.0052(1)	0.0044(1)
Cs(2)	0.00176(5)	0.00371(6)	0.0142(2)	0.00169(8)	0.0017(4)	−0.0032(4)
Mo(1)	0.00107(4)	0.00081(4)	0.00159(8)	0.00118(6)	0	0
Mo(2)	0.00186(3)	0.00128(3)	0.00203(5)	0.00221(4)	0.0009(1)	0.00084(9)
P(1)	0.0006(1)	0.0019(2)	0.0023(3)	0.0011(2)	0	0
P(2)	0.00160(9)	0.00121(9)	0.0013(2)	0.0018(1)	0.0007(3)	0.0004(3)
P(3)	0.0012(3)	0.0012(3)	0.0030(9)	0.0012(3)	0	0
P(4)	0.0012(3)	0.0012(3)	0.0048(9)	0.0012(3)	0	0
Al	0.0018(2)	0.0015(2)	0.0011(3)	0.0026(2)	0	0
			$K_4Cs_5Mo_9Al_3P_{11}O_{59}$			
K_2C_1	0.0086(1)	0.00497(7)	0.0048(2)	0.0109(1)	0.0070(3)	0.0058(2)
Cs(2)	0.00228(9)	0.0065(1)	0.0220(5)	0.0022(2)	0.0024(5)	−0.0109(6)
Mo(1)	0.00205(6)	0.00154(5)	0.0022(1)	0.00277(8)	0	0
Mo(2)	0.00404(5)	0.00221(4)	0.00394(9)	0.00466(6)	0.0029(2)	0.0024(2)
P(1)	0.0005(2)	0.0037(3)	0.0031(5)	0.0011(3)	0	0
P(2)	0.0028(1)	0.0021(1)	0.0017(3)	0.0035(2)	0.0006(4)	0.0009(4)
P(3)	0.0014(3)	0.0014(3)	0	0.0014(3)	0	0
P(4)	0.0023(4)	0.0023(4)	0.002(1)	0.0023(4)	0	0
Al	0.0028(2)	0.0023(2)	0.0020(5)	0.0041(3)	0	0
			$Rb_9Mo_9Al_3P_{11}O_{59}$			
Rb(1)	0.00691(9)	0.00486(8)	0.0068(2)	0.0088(1)	0.0071(2)	0.0063(2)
Rb(2a)	0.0038(4)	0.0085(6)	0.006(1)	0.0034(8)	0.0021(8)	−0.002(1)
Rb(2b)	0.0028(4)	0.0064(5)	0.015(1)	0.0021(7)	0.002(1)	−0.009(1)
Rb(3)	0.0047(7)	0.0047(7)	0.010(2)	0.0047(7)	0	0
Mo(1)	0.00237(8)	0.00178(7)	0.0036(2)	0.0027(1)	0	0
Mo92a)	0.0036(1)	0.0023(1)	0.0036(2)	0.0037(2)	0.0021(3)	0.0025(3)
Mo(2b)	0.0040(1)	0.00148(9)	0.0047(2)	0.0036(2)	0.0004(4)	−0.0002(3)
P(1)	0.0013(3)	0.0067(5)	0.0018(5)	0.0017(5)	0	0
P(2)	0.0033(2)	0.0022(2)	0.0027(3)	0.0032(2)	0.0009(5)	0.0008(5)
P(3)	0.0004(4)	0.0004(4)	0.007(2)	0.0004(4)	0	0
P(4)	0.0055(8)	0.0055(8)	0.003(1)	0.0055(8)	0	0
Al	0.0087(4)	0.0040(3)	0.0005(5)	0.0105(4)	0	0

[a] The form of the anisotropic displacement parameter is $\exp[-(\beta_{11}h^2 + \beta_{22}k^2 + \beta_{33}l^2 + \beta_{12}hk + \beta_{13}hl + \beta_{23}kl)]$.

Table 7. Coordinates and Occupancy of the Cationic Sites

compounds	sites		x	y	z	no. of atom per cell ($Z = 2$)
$Cs_9Mo_9Al_3P_{11}O_{59}$	I	Cs(1)	0.147	0.528	0.454	12
	II	Cs(2)	0.027	0.198	0.264	6
$Rb_9Mo_9Al_3P_{11}O_{59}$	I	Rb(1)	0.151	0.532	0.458	11.4
	II	Rb(2a)	0.030	0.215	0.281	3
		Rb(2b)	0.038	0.180	0.354	3
	III	Rb(3)	0.0	0.0	0.5	0.6
$K_2Cs_7Mo_9Al_3P_{11}O_{59}$	I	K_1C_2	0.146	0.527	0.452	12
	II	Cs(2)	0.027	0.198	0.263	6
$K_4Cs_5Mo_9Al_3P_{11}O_{59}$	I	K_2C_1	0.144	0.526	0.452	12
	II	Cs(2)	0.029	0.201	0.268	6

and $K_4Cs_5Mo_9Al_3P_{11}O_{59}$, in agreement with the smaller size of K^+ compared to Cs^+. In these sites labeled A_1 (Table 7), potassium and cesium ions are distributed at random. Note, however, that a complete occupancy of this site by potassium does not seem to be possible, since the phase $K_6Cs_3Mo_9Al_3P_{11}O_{59}$ could not be synthesized to date. This is in agreement with the A_1−O distances (Table 8), ranging from 2.79 to 3.34 Å, which are for most of them significantly larger than the sum of the ionic radii according to Shannon.[6] This explains the thermal B_{eq} factor of A_1, ranging from 3 to 3.9 Å^2, significantly larger than that of Cs(1) (2.8 Å^2).

In the same way, the presence of a big cation in the second site, labeled A_2, which corresponds to the large 12-sided tunnels, is absolutely necessary to stabilize this structure. This tunnel is indeed exclusively occupied by cesium or rubidium. Nevertheless, there is a fundamental difference between the Cs−aluminophosphates and the Rb−aluminophosphate. In the case of $Cs_9Mo_9Al_3P_{11}O_{59}$, $K_4Cs_5Mo_9Al_3P_{11}O_{59}$, and $K_2Cs_7Mo_9Al_3P_{11}O_{59}$, the A_2 site is half-occupied by Cs^+, whereas in $Rb_9Mo_9Al_3P_{11}O_{59}$ two Rb(2) sites exist, each of them one-quarter occupied by Rb^+; moreover, the Rb−aluminophosphate exhibits a third site A_3 that is 30% occupied by rubidium. The Cs(2)−O distances, ranging from 3.11 to 3.43 Å in the three compounds $Cs_9Mo_9Al_3P_{11}O_{59}$,[4] $K_2Cs_7Mo_9Al_3P_{11}O_{59}$, and $K_4Cs_5Mo_9Al_3P_{11}O_{59}$, do not vary significantly from one phase to the other. These large Cs−O distances, greater than the sum of the ionic radii of cesium and oxygen,[6] explain the rather high B_{eq} factors obtained for these phases (3.7, 4.4, and 7 Å^2, respectively). In fact the anisotropic thermal factors of these cations (Table 6, Figure 2) show that the thermal motion is principally directed along the axis of the large tunnel but also extended toward the A_1 site and increases as the Cs content decreases, in agreement with the larger space left by potassium.

The large size of the second tunnel explains the particular behavior of $Rb_9Mo_9Al_3P_{11}O_{59}$. Indeed, the study of the anisotropic thermal factors of Rb(2) (Figure 3a) showed that its agitation was principally directed along $\vec{c}$ (i.e., parallel to the axis of the large tunnel). This led us to consider two Rb(2) sites instead of one, labeled 2a and 2b. Due to its smaller size, the rubidium cation of these sites has moved away from the $z \approx 1/4$ mirror, so that two Rb(2) sites are one-quarter occupied (Table 3), with z parameters of 0.280 and 0.354, respectively, instead of one Cs(2) site half-occupied (with $z \approx 0.264$−0.268) in the Cs and K−Cs aluminophosphates. This "splitting" of the Rb(2) site allows smaller

(5) Zachariasen, W. H. *J. Less Common Met.* **1978**, *62*, 1.
(6) Shannon, R. P. *Acta Crystallogr.* **1976**, *A32*, 751.

Table 8. Cation–Oxygen Distances

	$K_2Cs_7Mo_9Al_3P_{11}O_{59}$		
K_1C_2–O(1)	3.223(9)	Cs(2)–O(1)	3.12(1)
K_1C_2–O(2vi)	3.34(1)	Cs(2)–O(3)	3.34(1)
K_1C_2–O(4)	3.292(9)	Cs(2)–O(6)	3.22(2)
K_1C_2–O(4vi)	3.065(8)	Cs(2)–O(6ix)	3.29(2)
K_1C_2–O(5vi)	3.127(8)	Cs(2)–O(6i)	3.37(2)
K_1C_2–O(8viii)	3.27(1)	Cs(2)–O(6x)	3.43(2)
K_1C_2–O(10viii)	2.851(9)	Cs(2)–O(7viii)	3.39(3)
K_1C_2–O(13iii)	2.899(6)	Cs(2)–O(9ix)	3.11(1)
K_1C_2–O(15)	3.20(2)		
	$K_4Cs_5Mo_9Al_3P_{11}O_{59}$		
K_2C_1–O(1)	3.18(2)	Cs(2)–O(1)	3.13(2)
K_2C_1–O(2vi)	3.29(2)	Cs(2)–O(3)	3.33(2)
K_2C_1–O(4)	3.30(2)	Cs(2)–O(6)	3.23(2)
K_2C_1–O(4vi)	3.02(2)	Cs(2)–O(6ix)	3.24(2)
K_2C_1–O(5vi)	3.08(1)	Cs(2)–O(6i)	3.41(2)
K_2C_1–O(8viii)	3.22(2)	Cs(2)–O(6x)	3.43(2)
K_2C_1–O(10viii)	2.79(2)	Cs(2)–O(7viii)	3.35(2)
K_2C_1–O(13iii)	2.93(1)	Cs(2)–O(9ix)	3.14(2)
K_2C_1–O(15)	3.14(2)		
	$Rb_9Mo_9Al_3P_{11}O_{59}$		
Rb(1)–O(1)	3.35(2)	Rb(3)–O(6a)	3.12(4)
Rb(1)–O(2vi)	3.37(3)	Rb(3)–O(6aii)	3.12(4)
Rb(1)–O(4)	3.23(2)	Rb(3)–O(6aviii)	3.12(4)
Rb(1)–O(4vi)	2.93(2)	Rb(3)–O(6aix)	3.12(4)
Rb(1)–O(5vi)	3.14(2)	Rb(3)–O(6axi)	3.12(4)
Rb(1)–O(8viii)	3.12(2)	Rb(3)–O(6axii)	3.12(4)
Rb(1)–O(10viii)	2.80(2)	Rb(3)–O(6b)	2.95(5)
Rb(1)–O(13iii)	2.80(1)	Rb(3)–O(6bii)	2.95(5)
Rb(1)–O(15)	3.07(3)	Rb(3)–O(6bviii)	2.95(5)
		Rb(3)–O(6bix)	2.95(5)
		Rb(3)–O(6bxi)	2.95(5)
		Rb(3)–O(6bxii)	2.95(5)
Rb(2a)–O(1)	2.78(3)	Rb(2b)–O(1)	3.43(3)
Rb(2a)–O(3)	3.31(2)	Rb(2b)–O(3)	3.42(2)
Rb(2a)–O(6aix)	3.19(4)	Rb(2b)–O(6a)	2.88(5)
Rb(2a)–O(6b)	2.98(5)	Rb(2b)–O(6aix)	2.87(4)
Rb(2a)–O(6bi)	3.32(5)	Rb(2b)–O(6viii)	3.23(4)
Rb(2a)–O(7viii)	3.16(2)	Rb(2b)–O(6b)	2.25(5)
Rb(2a)–O(9ix)	3.16(4)	Rb(2b)–O(6bix)	3.07(5)
		Rb(2b)–O(6bviii)	3.31(5)
		Rb(2b)–O(7viii)	2.98(2)
		Rb(2b)–O(8)	3.18(3)

Symmetry Code

i: $x; y; 1/2 - z$	vii: $1 - y; x - y; z$
ii: $y; y - x; 1 - z$	viii: $x - y; x; 1 - z$
iii: $1 - x; 1 - y; 1 - z$	ix: $-y; x - y; z$
iv: $1 + x - y; x; 1 - z$	x: $-y; x - y; 1/2 - z$
v: $1 - y; 1 + x - y; z$	xi: $-x; -y; 1 - z$
vi: $y - x; 1 - x; z$	xii: $y - x; -x; z$

Rb–O distances of 2.694–2.721 Å to be reached (Table 8); nevertheless, most of the Rb–O distances remain much larger than the sum of the ionic radii. This explains again the fact that the B_{eq} factors of Rb(2) remain relatively high, ranging from 5.0 to 5.8 Å^2 (Table 3). The anisotropic thermal factors (Table 6, Figure 3b,c) show that the Rb(2) atom has a motion similar to that of the Cs(2) atoms in the other compounds, but some differences appear between Rb(2a) and Rb(2b). The first one moves principally toward the A1 site whereas the second one runs along the axis of the tunnel. Finally the rubidium phase differs from the three other aluminophosphates by the fact that the Rb(3) site located in the large tunnels is 30% occupied, whereas it is empty in the other compounds. The Rb(3) atom exhibits in fact a trigonal antiprismatic coordination with six oxygen atoms at 3.12 Å (Table 8). These large Rb–O distances, greater than the sum of the ionic radii, are in agreement with the high isotropic factor of 4.6 Å^2.

The behavior of Rb(2) and Rb(3) in the tunnels indicates some possibility of ionic conduction along *c* in the $Rb_xCs_{9-x}Mo_9Al_3P_{11}O_{59}$ compounds that are very rich in rubidium. Unfortunately, problems with the samples sintering had not allowed us to verify the ionic conduction up to now.

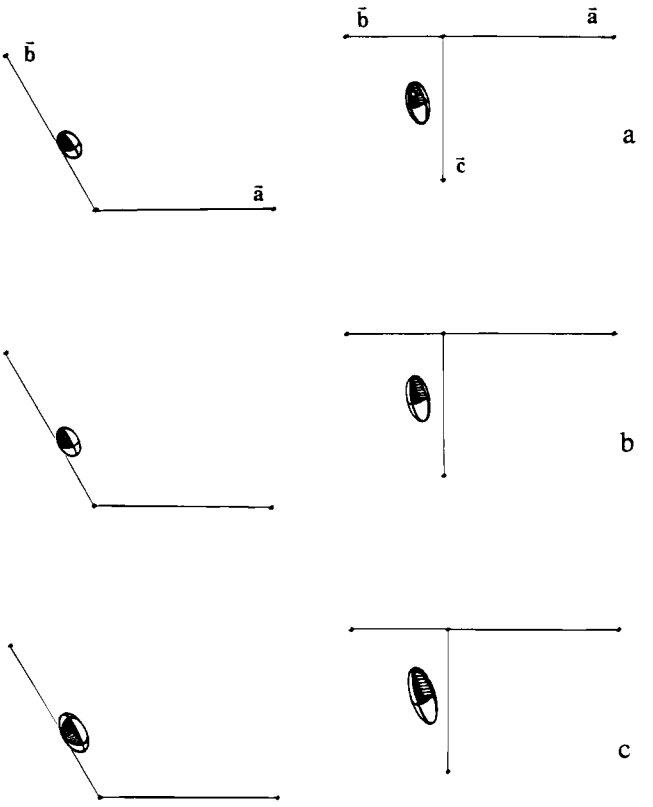

Figure 2. Thermal motion ellipsoids of Cs(2) in (a) $Cs_9Mo_9Al_3P_{11}O_{59}$, (b) $K_2Cs_7Mo_9Al_3P_{11}O_{59}$, and (c) $K_4Cs_5Mo_9Al_3P_{11}O_{59}$.

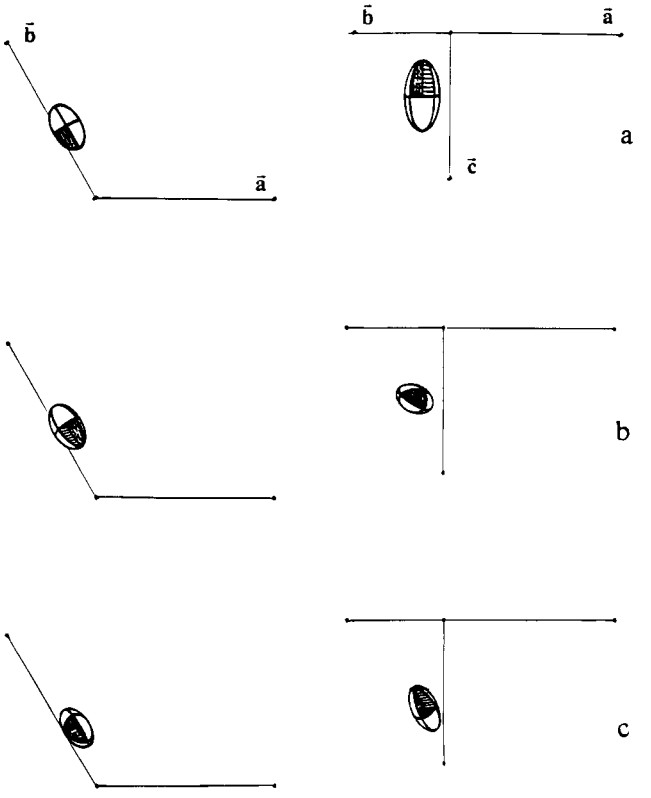

Figure 3. Thermal motion ellipsoids in $Rb_9Mo_9Al_3P_{11}O_{59}$: (a) of Rb(2) before its splitting into two sites: Rb(2a) and Rb(2b); (b) of Rb(2a); (c) of Rb(2b).

In conclusion, this structural study shows the great flexibility of the $[Mo_9Al_3P_{11}O_{59}]_\infty$ framework that can accommodate various cations. Nevertheless, the substitution of smaller cations for cesium induces significant disorganisation of this host lattice, which may be explained by various tiltings of the chains of polyhedra. It is most likely that all the high thermal factors that are observed here correspond in fact to a series of split positions of the atoms, due to very close configurations of the different chains of polyhedra. In the same way, it is not possible to distinguish between a true thermal agitation and very closely split positions for the various interpolated cations. But there is no doubt that the degree of disorganization is strongly correlated to the size of the interpolated cation. This disorganization may allow ionic conductivity through the tunnels.

Supporting Information Available: Crystal structure factors (25 pages). Ordering information is given on any current masthead page.

CM950118S